Transient heat flux estimation during the baking of cereal batter by contact heating

S. Marc, J.-P. Ploteau, P. Le Bideau, P. Glouannec

Version of Record: https://www.sciencedirect.com/science/article/pii/S0017931019365019
Manuscript_0695327116554305cf4df43d1696e266

Transient heat flux estimation during the baking of cereal batter by contact heating

S. Marc[a], J-P. Ploteau[a], P. Le Bideau[a,*], P. Glouannec[a]

[a] *Univ. Bretagne Sud, IRDL, UMR CNRS 6027, F-56100, Lorient, France*

Abstract

In many applications, it is essential to evaluate the heat flux transferred by contact between two materials. Heat flux sensors must be properly designed to reduce sources of measurement bias while maintaining a high sensitivity without disrupting the flux itself. The aim of this study is to estimate the heat flux exchanged between two materials in contact at different temperatures. When materials are rapidly brought into contact (less than one second) the heat flux exchanged presents large variations. In this study, the heat fluxes transferred are computed using an inverse heat conduction problem. Initially, a particular attention is focused on the numerical analysis of the method and its reliability. A first experimental study is conducted on a prototype where an elastomer plate is suddenly placed on a hot iron disk. Based on temperature measurements recorded in each medium, the heat flux exchanged is estimated by two ways and the results are compared with each other. These first results show the efficiency of the method and its ability to extract information from temperature measurements. Then, a second experimental study is carried out with a cereal batter spread on the iron disk.

*Corresponding author: pascal.le-bideau@univ-ubs.fr,+332.97.87.45.14

The estimation of the heat flux from cast iron temperatures is compared with that deduced from an energy balance performed on the batter. The energy balance takes into account the sensible heat, the mass losses and the heat flux exchanged by radiation and convection with ambiance.
Keywords: Direct contact heating, Inverse Heat Conduction Problem, Experiment, Heat flux density, Baking, Experimental test bench

---

Nomenclature

Normal

c_p	specific heat $\mathrm{J{\cdot}kg^{-1}{\cdot}K^{-1}}$
h	convective heat transfer coefficient $\mathrm{W{\cdot}m^{-2}{\cdot}K^{-1}}$
k	thermal conductivity $\mathrm{W{\cdot}m^{-1}{\cdot}K^{-1}}$
L_v	latent heat $\mathrm{J{\cdot}kg^{-1}}$
m	masse kg
R_c	thermal contact resistance $\mathrm{m^2{\cdot}K{\cdot}W^{-1}}$
T	temperature K

Greek letters

α	thermal diffusivity $\mathrm{m^2{\cdot}s^{-1}}$
ϵ	emissivity
ρ	density $\mathrm{kg{\cdot}m^{-3}}$
σ	Stefan Boltzmann constant $\mathrm{W{\cdot}m^{-2}{\cdot}K^{-4}}$
φ	heat flux $\mathrm{W{\cdot}m^{-2}}$

Subscripts

amb	ambient
ci	cast iron
cond	conduction
conv	convection
e	elastomer
exp	experimental
imp	imposed
m	metallic mass
pyro	pyrometer
rad	radiation

1. Introduction

The optimization of cooking appliances is becoming a priority for many sectors of the food processing industry [1–4] such as for cooking systems by contact [5]. Heating or cooling by direct conduction can involve high heat transfers. This cooking method is widespread around the world [6, 7] but knowledge in this field is generally empirical and based on know-how rather than on technical and scientific knowledge. In the case of cooking where a product, whose initial temperature can be between −30 °C and room temperature, is placed directly on a hot metal plate between 100 °C and 300 °C , it is essential to know the heat flux transferred from the hot surface to the product to optimize the heating system and control the quality of the end

product [8]. A non-exhaustive literature survey reveals that many studies focused on the estimation of heat fluxes exchanged during the contact of two products initially at different temperatures. Some of them rest on the cooking processes [9–12] but a large amount of these studies dealt with other fields such as metallurgy [13, 14], plastics [15] and glasswork [16]. For all these processes, the heat flux transferred, which is a function of the thermal contact resistance and contact temperatures, can vary greatly. For industrial productions, a perfect knowledge of heat flux and contact resistances is required to ensure the quality and the repeatability of the production. The estimation of heat flux, contact resistances or contact temperatures can be performed by solving an Inverse Heat Conduction Problem (IHCP) [17]. Many studies have been conducted in recent years to solve different problems that can be mathematical [18] or more applied such as controlling the occurrence of irregularity in heat curing composites [19], heat flux identification in a reduced scale braking system [20] and the estimation of the incident radiant heat flux in an infrared oven [21]. In the field of cooking by direct conduction, Sanz-Serrano [22] proposed a study on the estimation of power distribution in a pan by analyzing surface temperatures and using an inverse model according to different heating systems: induction, electric resistance and gas. However, whatever the configurations, the pan is considered empty, without any food, that which could not be representative of the real heat flux transferred from the pan to the foodstuff.

The purpose of this article is to present a methodology to design a heat flux sensor composed of a metallic mass instrumented with thermocouples and directly integrable inside a hot plate. The procedure rests on

Inverse Heat Conduction Problem (IHCP). In the first part of this article, the methodology used is described. A 2D numerical model is developed and the conditions for optimal instrumentation for the resolution of the inverse heat conduction problem are presented. A description of the characterization of the thermophysical properties of the materials used is then given. Subsequently, the numerical results are discussed. A sensitivity analysis is performed to quantify the impact of materials properties and sensors location on the estimation. Finally, experiments are carried out to evaluate the estimation method on the basis of real measurements.

Two configurations have been studied, the first one with an elastomer to simulate the future presence of the batter, but with a medium not subjected to shrinking and the second one corresponding to the baking experiment. First tests are performed with an elastomer plate in order to calibrate and validate the transient method and avoid approximations relating to food products, such as encountered by Cernela [8]. Then, the proven method is used to estimate heat flux transmitted to a cereal batter during its cooking.

2. Problem statement and numerical development

The objective of the study is to measure the transient heat flux transferred from a hot metallic surface to a product placed in contact with it (figure 1). A heat flux sensor is embedded in the metallic plate and designed to be as non-intrusive as possible. The heat flux sensor consists of a metallic cylinder previously instrumented with thermocouples. The method is based on the resolution of an Inverse Heat Conduction Problem (IHCP) for the estimation of heat flux from temperature measurements. The procedure is tested and

validated for two configurations where either an elastomer plate or a cereal batter at room temperature, is placed on or spread over the hot surface.

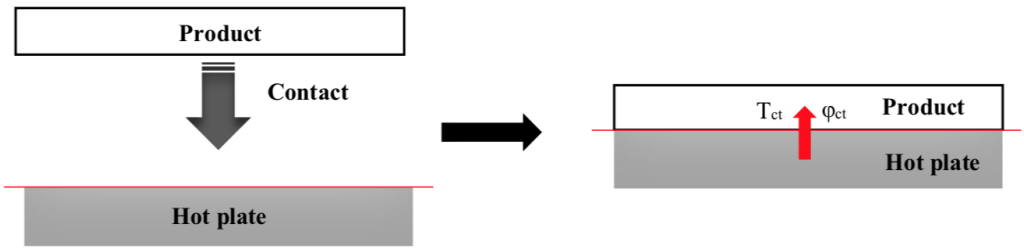

Figure 1: Schematic description of the study

Numerical and experimental studies are first conducted with an elastomer plate to design the heat flux sensor. An axisymmetric 2D Finite Element Model is developed to simulate the heat flux at the elastomer/cast iron interface. Simulations are performed, taking into consideration that the thermal contact is not perfect and the contact time not instantaneous [17]. The media are supposed homogeneous. The comparison is made between the heat flux deduced from 2D model and the heat flux obtained by the resolution of an IHCP based on the temperature variations of the 2D model to validate the 1D assumption of the direct problem. Then, the objective is to study the ability of the method to estimate a known 1D heat flux and to test its sensitivity.

2.1. 2D numerical model applied to elastomer plate

The description of the study with the elastomer is given in figure 2. A metallic mass stuck on the elastomer permits creating a heat sink and maintaining constant pressure after contact with the hot plate during the experimental tests. A perfect thermal contact is assumed between the metallic

mass and the elastomer (z = 8 mm). The upper and lateral surfaces of these two materials and the thermal insulation are subjected to thermal exchanges by natural convection and thermal radiation.

A time varying contact resistance R_c is introduced (z = 0) to take into account the roughness and the non-instantaneous contact between the elastomer and cast iron. More details about the variation of the contact resistance are given in the subsection 3.3. The temperature of the bottom surface of the cast iron (z = -15 mm) is assumed to be constant throughout the simulation. The air and wall temperatures are also constant.

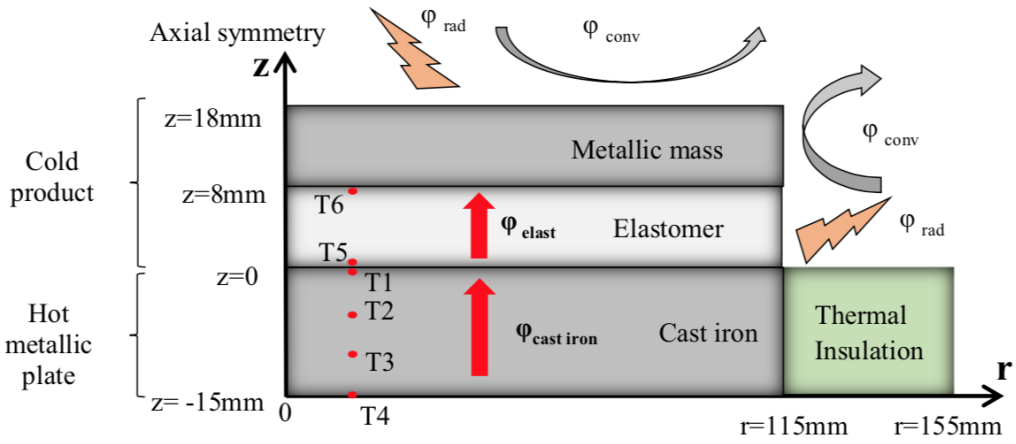

Figure 2: Schematic description of the 2D axisymmetric model

In the cast iron, the elastomer and the metallic mass, the governing equation is:

$$\rho c_p \frac{\partial T}{\partial t} + \nabla \left(-k \nabla T\right) = 0 \tag{1}$$

The conductivities and thermal capacities of the cast iron and the elastomer are functions of the temperature (figure 3). The boundary conditions

are the following:

- Interface between the air and the metallic mass, the elastomer and the thermal insulation:

$$-k_{e,m}\frac{\partial T_{e,m}}{\partial z} = \varphi_{rad} + \varphi_{conv} \tag{2}$$

φ_{rad} is the radiative heat flux between the materials surfaces and surrounding walls considered as a black surface at ambient air temperature:

$$\varphi_{rad} = \epsilon_{e,m}\sigma\left(T_{e,m}^4 - T_{wall}^4\right) \tag{3}$$

φ_{conv} is the convective heat flux. Free convection correlations for the horizontal plate (z=18 mm) and for the vertical surface (r=115 mm) are used.

$$\varphi_{conv} = h_{conv}\left(T_{e,m} - T_{wall}\right) \tag{4}$$

- Interface between the metallic mass and the elastomer (z=8mm):

$$-k_e\frac{\partial T_e}{\partial z} = -k_m\frac{\partial T_m}{\partial z} \tag{5}$$

- Interface between the elastomer and the cast iron (z=0+):

$$-k_e\frac{\partial T_e}{\partial z} = \frac{T_{ci} - T_e}{R_c} \tag{6}$$

- Interface between the cast iron and the elastomer (z=0-):

$$-k_{ci}\frac{\partial T_{ci}}{\partial z} = \frac{T_{ci} - T_e}{R_c} \tag{7}$$

- Bottom of the cast iron (z=-15mm):

$$T_{ci} = T_{imp} \tag{8}$$

Where ci, e and m correspond to cast iron, elastomer and metallic mass, respectively. R_c is the thermal contact resistance and T_{imp} is the imposed temperature.

This model permits calculating the heat flux exchanged at the interface between the cast iron and the elastomer ($\varphi_{2D\,model}$) based on equations 6 and 7. This heat flux will be used as a point of comparison in the following numerical study of IHCP.

2.2. IHCP one dimension

The problem consists in estimating the heat flux at the interface between cast iron and elastomer (z = 0) using the temperature recorded in different positions in the two materials.

Two IHCP are solved separately: one in the cast iron and the second in the elastomer. Considering a one-dimensional problem in the central part of the plates, the heat equation therefore takes the following form:

$$\rho c_p \frac{\partial T}{\partial t} = k \frac{\partial^2 T}{\partial z^2} \tag{9}$$

The thermophysical properties are a function of the temperature (1) and the boundary conditions are the following:

$$z = 0 \qquad -k_{ci,e} \frac{\partial T_{ci,e}}{\partial z} = \varphi \tag{10}$$

$$z = -15\text{mm} \qquad T_{ci} = T_{imp1} \tag{11}$$

$$z = 8\text{mm} \qquad T_e = T_{imp2} \tag{12}$$

The equations are solved by a pure implicit method. In order to obtain an acceptable sensitivity, the location of the sensors $T2$ and $T5$ must be determined precisely and conform to the criteria described in the literature [23, 24]. The noise measurement must be mastered in order to limit its amplification. A deep implantation was chosen using the following criteria [23]:

$$1 > \Delta t_i > 10^{-2} \tag{13}$$

with Δt_i the characteristic time step: $\Delta t_i = \dfrac{\alpha \Delta t}{E^2}$

Δt being the time discretization of the numerical model (s), α the thermal diffusivity ($\text{m}^2 \cdot \text{s}^{-1}$) and E the distance between the temperature sensor and the contact surface. The value of Δt must be chosen such that the temperature variation during the step time is greater than the measurement noise δT:

$$\frac{T(z_j, t + \Delta t) - T(z_j, t)}{\delta T} >> 1 \tag{14}$$

Thermocouples must be accurately positioned to meet the following condition:

$$\frac{\delta z}{d} < 0.05 \tag{15}$$

Where δz is the error on the thermocouple position and d the distance between the contact surface and the closest sensor.

The heat flux is then determined using a procedure which minimizes a quadratic criterion [17] equal to the sum of squares of differences between the measured and computed temperatures at the selected spatial point. For each case, only one thermocouple located at d is used to estimate the heat flux:

$$S\left(\varphi(t)\right) = \frac{1}{2}\sum_{t=1}^{N}\left(T(d,t) - T_{exp}(d,t)\right)^2 \tag{16}$$

With N being the number of measurements and the subscript d refers to the location of the selected thermocouple.

This goal function is minimized using an iterative regularization method. A stopping criterion is imposed for the minimization procedure:

$$S\left(\varphi(t)^{fk}\right) = N\sigma^2 \tag{17}$$

With σ^2 is the noise variance due to temperature measurements and fk is the last iteration index.

The three criteria (13), (14) and (15) are taken into account to design the experimental device. In literature, the numerical tests are often carried out with academics signals like triangular, square or sin wave heat flux [25]. In this study, the contact heat flux varies considerably and quickly. An exponential decay of heat flux is expected. IHCPs are solved in the elastomer and the cast iron from the temperatures given by the 2D model to estimate the heat flux at the interface cast iron / elastomer. The two estimated heat fluxes, one by IHCP in the elastomer and the other by IHCP in the cast iron, are compared to validate the procedure and experimental design.

3. Experimental study

3.1. Thermo-physical properties

The thermal properties of the cast iron and the silicone elastomer were measured with various equipments indicated in table 1. Measurements of diffusivity and specific heat were performed on both materials, see figure 3. The expansion coefficient of the cast iron was also determined. The thermal conductivity was deduced from the thermal diffusivity, density and specific heat. The properties measured are in good agreement with those of the literature [26, 27].

Table 1: Thermal properties

Property	Method	Apparatus	Accuracy
$\rho(\mathrm{kg{\cdot}m^{-3}})$	Pycnometer Dilatometer	Mettler Toledo XS205 Linseis L75H	±4%
$c_p(\mathrm{J{\cdot}kg^{-1}{\cdot}K^{-1}})$	Calorimeter	Netzsch 204 F1 Phoenix	±3%
$\alpha(\mathrm{m^2{\cdot}s^{-1}})$	LFA	Netzsch LFA 457	±5%

3.2. Description of experimental set-up and instrumentation

A 23 cm diameter and 15 mm thick cast iron plate was used as hot surface. A hole was bored in the center of the plate so that an instrumented flux meter also made of cast iron could be inserted into the plate, see figure 4. Its diameter was 30 mm and it was held in position by a mechanical adjustment. It is considered here that the elevation of the plate's temperature would result in the expansion of the material and therefore tighten the contact flux meter/plate. Therefore, no contact resistance between these two materials was considered.

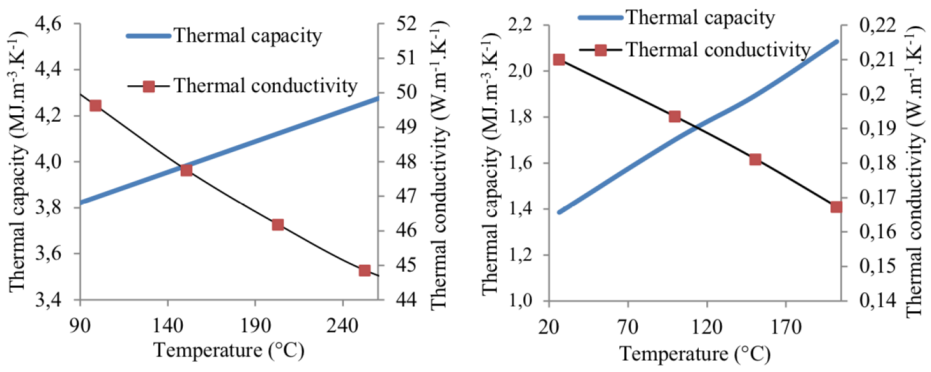

(a) (b)

Figure 3: Thermal capacity and thermal conductivity for cast iron (a) and elastomer (b)

In order to meet the criteria given in (13), the first thermocouple was located 3 mm from the surface (z = 0), assuming a time step $\Delta t = 0.1$ s for the IHCP.

At this position, the characteristic time was 0.14 s, which corresponds to the criteria (13) $1 > \Delta t_i > 10^{-2}$. Three K-type stainless steel jacketed thermocouples of 500 µm diameter were embedded at different depths: T2, T3 and T4 (figure 4). The thermocouple T2 was used as output to estimate the heat flux while the thermocouple T3, was taken into account as boundary conditions. These thermocouples were placed along the isotherms. In the 30 mm pellet, the bores were drilled at 90° from each other and are parallel to the expected isotherms. They had a length of 13 mm and a 4 mm space in radius direction between each bore is present in order to cause no interference.

A 250 µm diameter thermocouple T1 was located next to the flux meter. Due to its location, its measurement was not reliable but could quickly detect contact with a product. The time constant of the sensors and the contact resistance between the probes and the material were assumed negligible.

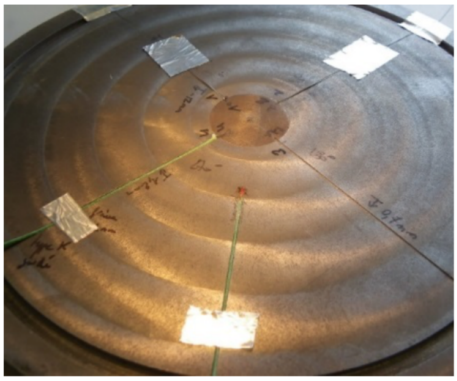

(a)

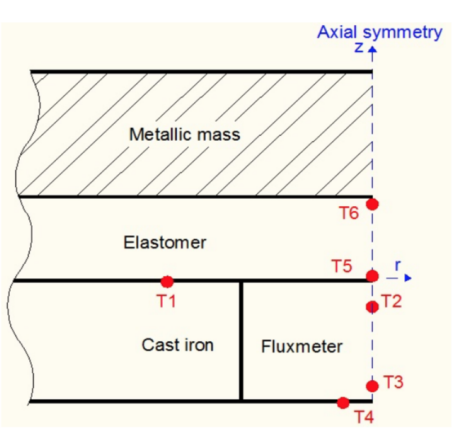

(b)

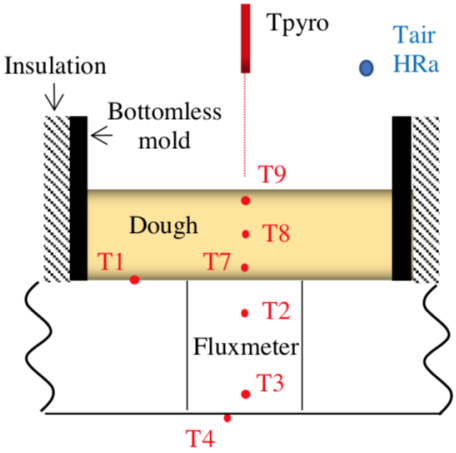

(c)

Figure 4: Instrumented fluxmeter (a) placed under an elastomer (b) or under dough (c)

A 23 cm diameter radiant hob was placed under the cast iron plate. The power supplied to this device is regulated by a solid-state relay (Eurotherm Epack) controlled by an analogical signal (Eurotherm 3216). The solid-state relay communicated via Ethernet with a desktop computer. The radiant hob / hot plate system was thermally insulated on the lateral sides and at the bottom by a high temperature insulating material made of calcium silicate.

The surface facing the heater was blackened by applying a uniform layer of graphite to obtain an emissivity of the plate close to black body emissivity. The contact surface was treated with a thin layer of burnt sunflower oil to enhance the contact.

Elastomer: In order to simulate the heating of a cold product, an 8 mm thick silicone elastomer was used. 80 µm diameter K-type thermocouples (weld of 160 µm) were located along the isotherms at a depth of 0.25 mm and 7.75 mm from the contact surface (table 2). The thermocouple T5 was used to estimate the heat flux while the thermocouple T6 was used as boundary conditions. The characteristic time was 0.21 s which also met the criteria (13). To ensure the contact elastomer/hot plate, a metallic mass was bonded to the elastomer and the assembly was placed on the heating surface for the tests. The metallic mass permitted maintaining contact pressure during testing.

Cereal batter: A PTFE bottomless mold of internal dimensions 14 x 11.5 x 2 cm, surrounded by thermal insulation, was placed on the surface of the cast iron plate. About 150 g of batter at room temperature was poured into the bottomless mold, which represents 8 mm thick (figure 4). Three temperatures were recorded by K-type thermocouples in the dough (T7, T8, T9). The

diameter of the thermocouples was 125 µm and a pyrometer measured the surface temperature. The mass loss was measured using a Radwag PS6000 R2 (accuracy 0.01 g). In addition, air temperature and relative humidity were also recorded. The batter used consisted of a mixture of an industrial preparation (Francine® mix) and sterilized semi-skimmed milk. The weight percentage used was 37 % mix and 63 % milk. The thermal properties were calculated with the correlations of Baik & al.[28] presented in appendix A. These correlations were used to consider the properties as functions of the temperature and the water content.

The z coordinates of the different thermocouples are indicated in table 2. The temperature measurements were performed by a QuantumX MX1609KB data acquisition system communicating with the desktop computer by Ethernet. The acquisition period was set at 20 ms.

Table 2: Implantation of thermocouples (mm)

Cast iron		Elastomer		Dough	
T1	0	T5	0.25	T7	1.0
T2	-3	T6	7.75	T8	4.0
T3	-12.5			T9	7.0
T4	-15				

3.3. Contact thermal resistance

When the product (elastomer or cereal batter) is placed or spread on the hot surface (cast iron disc), the contact cannot be considered instantaneous. Others authors like Beck [17] suppose a gradual contact which leads

to consider a decrease of contact resistance with time. A similar procedure was conducted here. Based on pictures obtained with a scanning electron microscope (figure 5), the surface roughness of the cast iron was observed to estimate the final air gap at the interface (between 50 µm and 100 µm). Thus, the final contact resistance is equivalent to thermal resistance caused by an air gap of this thickness or more. As Beck [17] a gradual contact in 0.3 s is assumed and a mathematical relation (polynomial form) with time was used to take into account this decrease with time (figure 6).

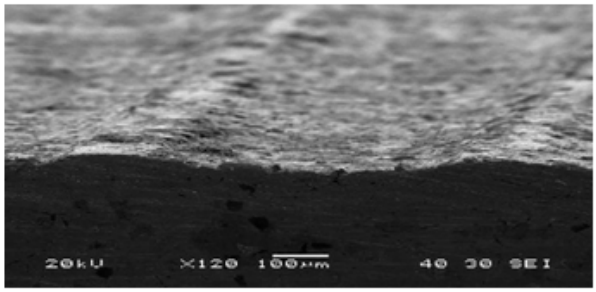

Figure 5: SEM view of the cast iron surface

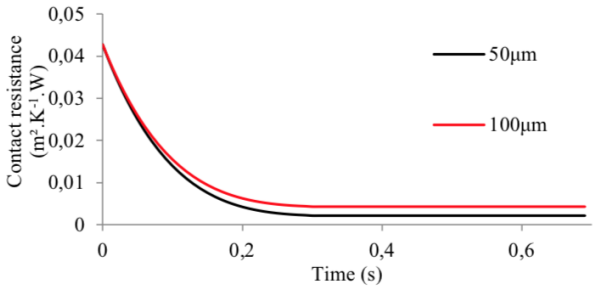

Figure 6: Contact resistances for air gaps of 50 µm and 100 µm

4. Results and discussion

In this section, the flux meter designed is tested. Firstly, the numerical results demonstrate the feasibility of the method and validate the IHCP. The experimental tests are then presented with an elastomer plate and a cereal dough.

4.1. Numerical studies

Two tests were conducted, the initial bottom surface temperature of the cast iron was imposed at 100 °C and 200 °C. The initial temperature of the elastomer was 20 °C. The gradual contact lasted 0.3 s as previously indicated and it was initialized at t = 1 s. The direct problem was solved with a step time of 20 ms corresponding to the maximum acquisition frequency.

4.1.1. 2D model simulation

The temperature variations in the cast iron and the elastomer are respectively presented in figure 7 a and b for the test performed at 100 °C. The thermal resistance in this instance is equivalent to an air gap of 100 µm. The heat flux at the contact surface calculated by the direct model is also plotted.

The temperatures near the contact surface varied significantly. The maximum temperature difference was higher than 60 °C in the elastomer, because of the low thermal conductivity. In contrast, in the cast iron, the temperature difference was rather weak, about 2 °C but the variations were still higher than the noise measurement obtained at 100 °C. For the tests at 200 °C, the temperature difference in the cast iron was 5.5 °C in the case of an air gap of 50 µm and 4.5 °C in the case of an air gap of 100 µm.

The impact of the mesh on the temperature evolutions was also studied and a satisfactory relationship between computation time and accuracy of the results was found. The Finite Element Model composed of 12 330 triangular elements.

Moreover, heat fluxes distributions with radius were investigated to check the uniformity of the interface heat flux. The figure 8 shows the heat flux distribution with radius r for selected times (before the contact, at the contact instant and after the contact instant). This plot is relating to the 2D heat transfer model as presented in figure 2. We note that the heat flux is globally constant with the radius in this configuration.

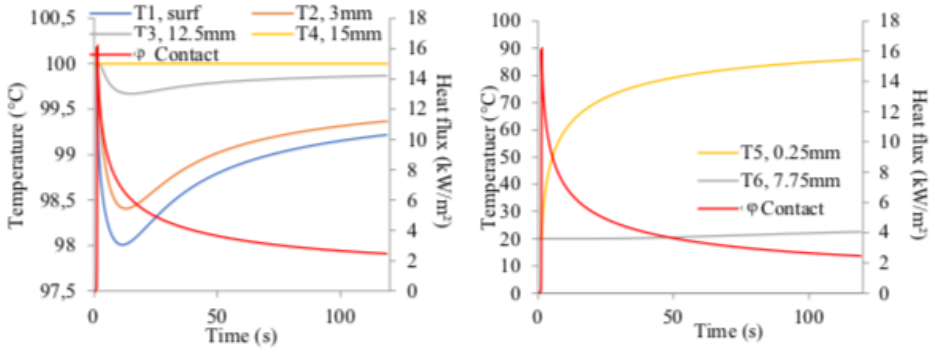

(a) Cast iron

(b) Elastomer

Figure 7: Numerical temperature evolutions and heat flux at the contact surface

4.1.2. IHCP estimation from the evolution of 2D temperature

In this part the 2D simulated temperatures were used to estimate the heat fluxes at the interface elastomer/cast iron by the inverse method. Before that, a sensitivity analysis was carried to check the feasibility of the estimation by an inverse procedure. Each value of heat flux estimated at a given time is

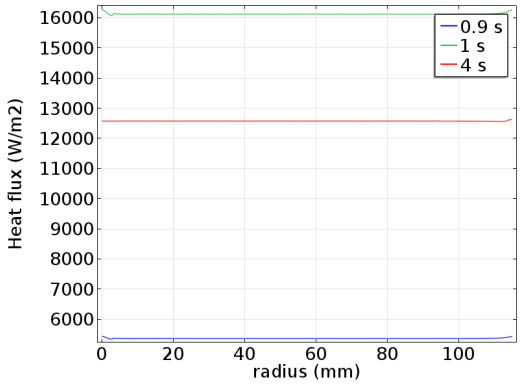

Figure 8: Heat flux distribution as function of radius

an independent parameter. No dependence between the parameters appears here as it's shown in the figure 9 which concerns the sensitivity analysis for the cast iron. This figure presents the sensitivity coefficients $\frac{\partial T}{\partial \varphi}$ vs time for the selected position (3 mm from the interface). The sensitivity coefficients plotted are those before the contact (φ_{bc}), at the instant of contact (φ_c) and after the contact (φ_{ac}). All sensitivity coefficients are the same trend ,i.e, a sudden peak immediately after the heat flux variation followed by a rapid decrease. Globally, no dependence between the signals appears.

Figure 10a shows the heat fluxes estimated by inverse techniques and calculated by the 2D model for the test at 100 °C, and for a final contact resistance equivalent to 100 µm. We observed good agreement between the three curves, except for the beginning of the estimation. Indeed, a "delay" on the estimation at the beginning of the flux was observed (t = 1 s). This phenomenon was visible in the first 0.3 seconds of the onset of flux (t = 1.3 s). However, for the rest of the estimation, the relative error was less than 2%. The resolution of the IHCP provide better accuracy if the calculation

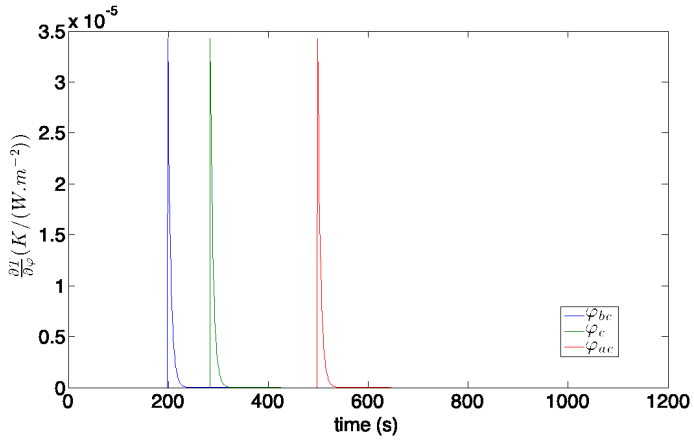

Figure 9: Sensitivity coefficients variations for a selected position (3 mm) in the cast iron.

time of IHCP is 0.1 s. From these results, the 1D assumption of the problem was validated.

The time step of the calculation used for the direct problem also affected the estimated heat flux. Indeed, an excessively long time step would result in a poor estimation in the first seconds of contact. Conversely, an excessively short time step would result in rebound phenomena due to the small temperature variations during the step time. After the first few seconds the influence of this step time was more negligible although disturbances could appear for a short step time (figure 10b).

The numerical analysis showed that the inverse method was able to re-estimate an imposed heat flux with satisfactory accuracy. Thereafter, a time step of 0.1 s was used.

A study of the impact of uncertainties on the thermo-physical properties and position of the thermocouples was conducted: 5% for thermal conductivity and heat capacity and 0.25 mm for the location of thermocouple. For

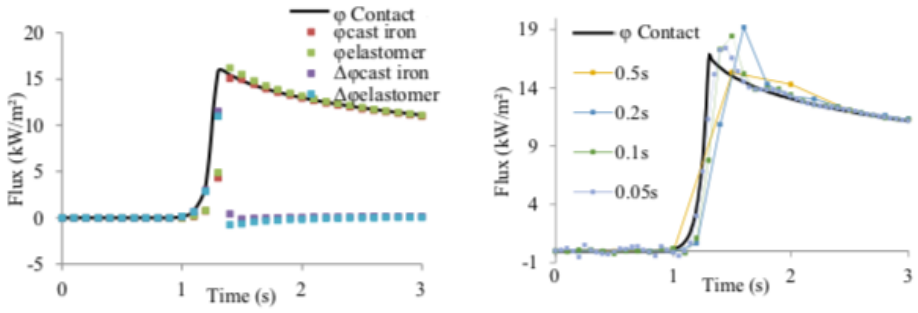

(a) (b)

Figure 10: (a) Comparison between heat fluxes computed by the 2D model and estimated by IHCP; (b) Influence of the step time on the estimation

this last point, the heat fluxes estimation were done with nodes located at 3.25 mm (instead of 3 mm) in the cast iron and at 0.5 mm (instead of 0.25 mm) in the elastomer. Figure 11 shows the differences between the heat flux imposed and estimated at the interface during the first eight seconds. The error on the estimation could be considerable at the beginning of contact (between t = 1 s and t = 2 s), mainly for the heat flux based on the cast iron temperatures and this, whatever the error source: properties uncertainties or sensors location. After 3 seconds, the errors tend to zero.

4.2. Experimental studies with elastomer

The cast iron plate was heated using a constant supply voltage of the infrared heating element. When the steady state was established, the elastomer was suddenly placed in contact on the cast iron plate. A metallic mass bonded to the upper face of the elastomer ensured constant pressure throughout the duration of the experiment in order to favour the repeatability of measurements. Temperatures were recorded every 20 ms. An average

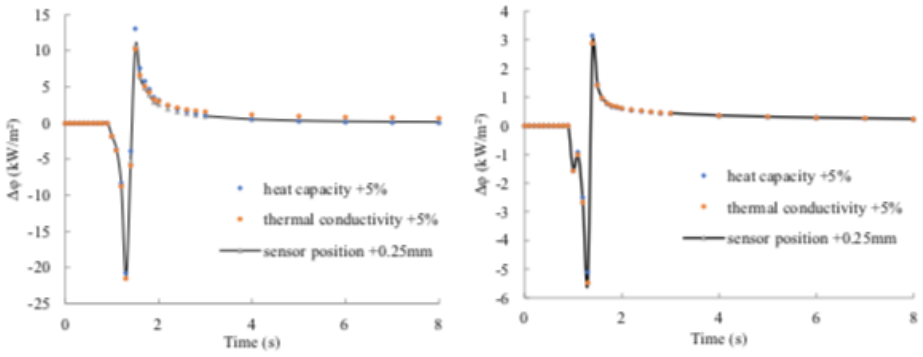

(a) (b)

Figure 11: Difference between fixed and estimated heat flux for thermal properties and sensor position errors: (a) cast iron, (b) elastomer

of 5 measurements were performed and stored every 0.1 s. This time step allowed a temperature variation greater than the measurement noise (14).

Firstly, the experiments performed with a fixed power of 140 W are described. In this case the lower surface of cast iron plate was initially at a temperature above 170 °C. The contact between the elastomer and the cast iron lasted 120 seconds. The temperatures recorded at 3 mm, 12,5 mm and 15 mm in cast iron are reported in figure 12a. A rapid drop in temperatures was visible as soon as the materials came into contact, with a temperature difference of about 4 °C between the sensors T2 and T4. In the elastomer, the temperature difference rapidly became greater than 100 °C (figure 12c).

Figure 12b and 12d shows another test performed for a power of 200 W, i.e. an initial cast iron temperature above 200 °C. In this case the temperature difference between the sensors T2 and T4 was about 6 °C.

Figure 13 shows that the heat fluxes estimated based on elastomer temperatures and cast iron temperatures are very similar in the temperature

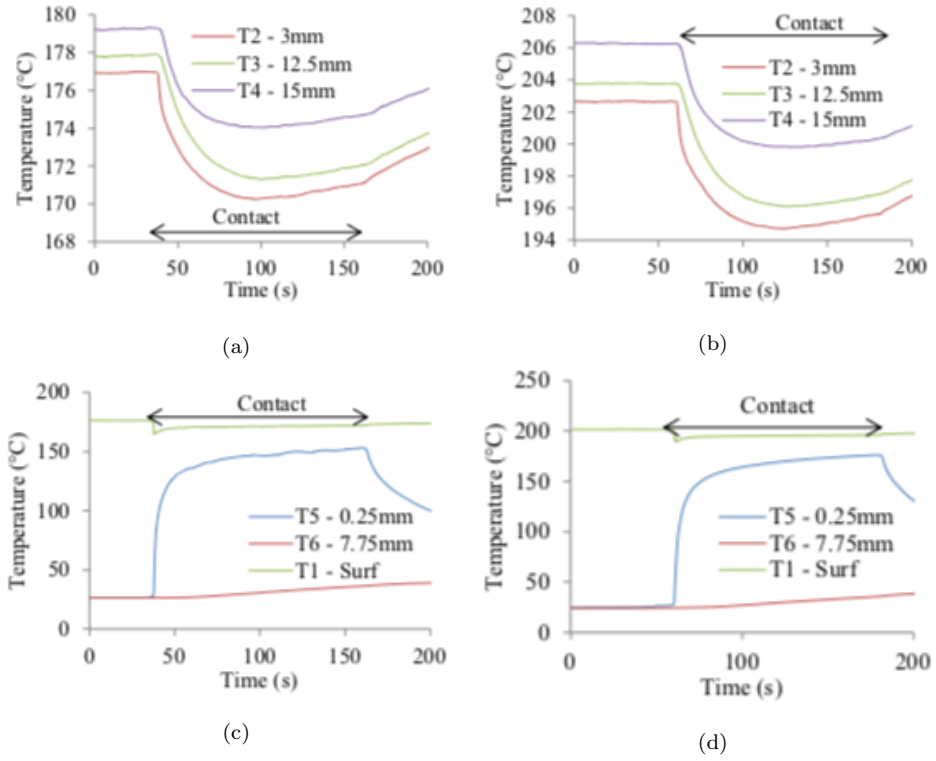

Figure 12: Temperatures of the cast iron (a, b) and elastomer (c, d) for initial cast iron temperatures of 170 °C and 200 °C

range studied. Based on the heat flux profiles, the contact duration was estimated at about 0.3 s. The estimation of the maximum peak was difficult during the first instant due to the weak thermal gradient in the cast iron. Logically, the higher the temperature of plate was, the higher the peak with a maximum at $42\,\mathrm{kW{\cdot}m^{-2}}$ for the test at $200\,^{\circ}\mathrm{C}$ against $35\,\mathrm{kW{\cdot}m^{-2}}$ for the test at $170\,^{\circ}\mathrm{C}$. Before the contact and after the elastomer withdrawal ($t > 130$ s), the heat flux estimated with cast iron temperatures corresponded to heat losses with the ambiance ($\approx 5\ \mathrm{kW{\cdot}m^{-2}}$). The procedure was repeated 4 times and error bars were added to the plots to underline the repeatability of the method. These results demonstrate the ability of the IHCP method to accurately estimate a heat flux transferred at the interface of two contacted materials. In fact, when the elastomer was suddenly brought into contact with the cast iron, the temperatures into the cast iron decreased although the temperature into the elastomer increased. The thermal responses were only due to the heat flux transferred and the own thermal properties of each material. It is possible to estimate by inverse method the trend and the values of this heat flux based on the temperature variation at a selected point and knowing with accuracy the thermal properties. Here, the heat flux was estimated by two means: one ICHP is solved in the cast iron and a second one is solved in the elastomer.

To estimate the contact thermal resistance, an additional test was performed for a time long enough to reach steady state (figure 14). The temperatures at the interface were calculated by the one-dimensional heat conduction model for the two materials at the end of the heat flux estimation. In steady state, the surface temperatures obtained numerically by the direct model

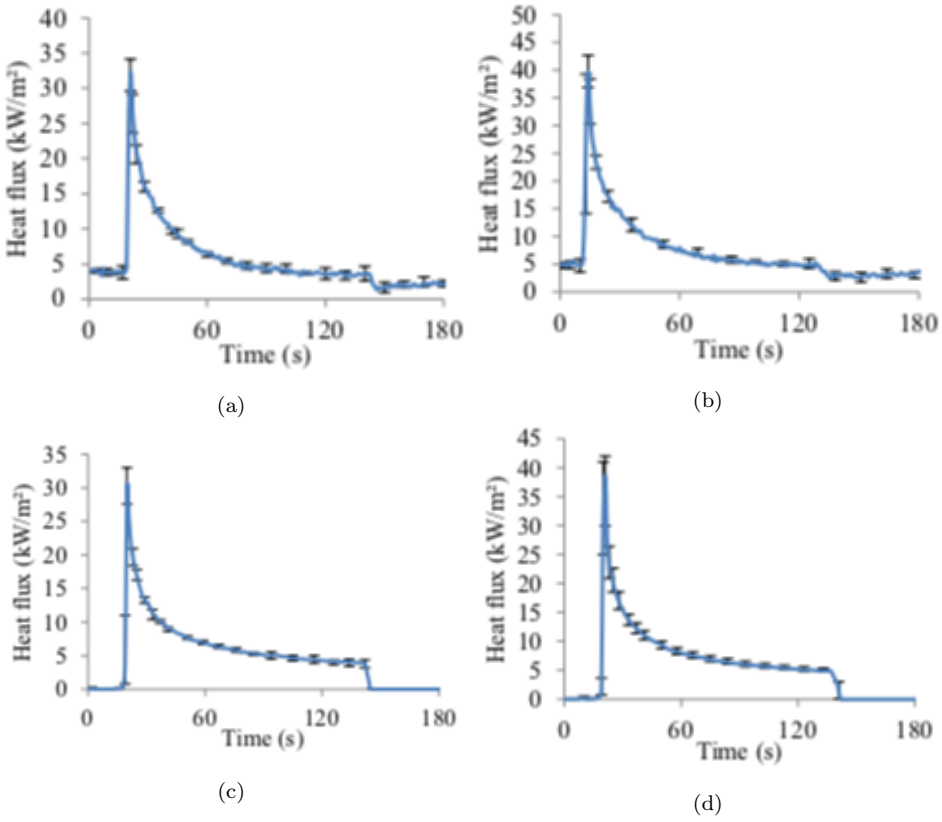

Figure 13: Comparison of estimated heat fluxes in cast iron (a-b) and elastomer (c-d) at 170 °C and 200 °C

were 198.2 °C and 187.1 °C for respectively the cast iron and the elastomer. Based on the heat flux estimated at 4.9 kW·m^{-2} and the interface temperatures, the contact resistance was calculated by the equation (18) after 220 s:

$$R_c = \frac{T_{\text{surf cast iron (z=0-)}} - T_{\text{surf elastomer (z=0+)}}}{\varphi} \tag{18}$$

A value of 2.3×10^{-3} m^2·K·W^{-1} was calculated. In this case, this thermal resistance value corresponded to an equivalent thermal resistance caused by a 53 µm air gap.

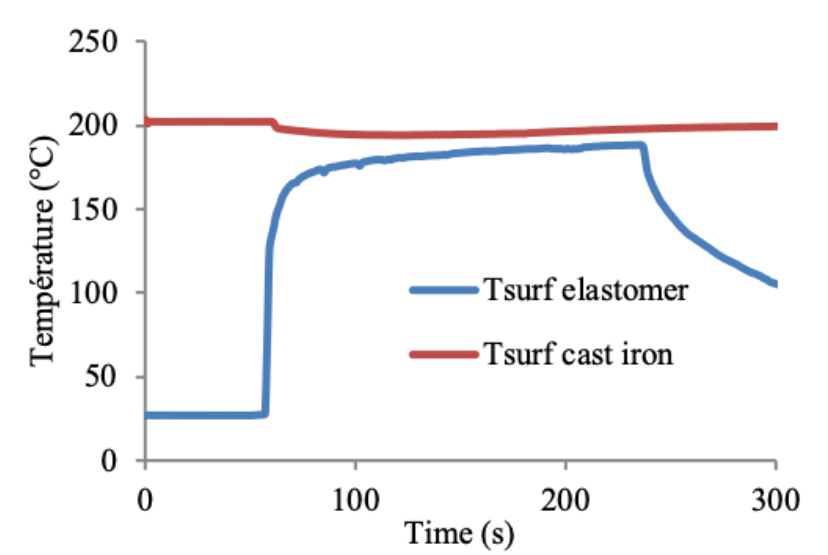

Figure 14: Temperature evolutions for the contact resistance estimation at 200 °C

4.3. Experimental tests with cereal dough

For this study, the temperature of the cast iron plate was regulated, and a set point of 200 °C was imposed for temperature T2. A bottomless PTFE mold surrounded by thermal insulation, was placed on the surface of the cast

iron plate. When steady state was reached, 150 ± 3 g of dough, initially at room temperature, was poured in the crucible, corresponding to a thickness of about 8 mm. The mass variation was continuously recorded by a precision balance, three temperature sensors were embedded into the dough (table 2) and air conditions were tracked.

In order to verify the repeatability of the measurements, this test was performed 3 times in the same experimental conditions. Figure 15 shows the temperatures measured within the dough during 20 minutes and the dimensionless mass obtained by mass monitoring. For the temperatures curves, the errorbars representing the maximum/minimum values are also plotted. The dough temperatures quickly increase and reach steady state after about 15 minutes. During this same duration, the mass losses represent approximately 15 % of the initial mass. A good repeatability is observed for the temperature measurements inside the dough and for the mass losses. The heat flux estimated by IHCP presents an initial peak of $35\,\mathrm{kW{\cdot}m^{-2}}$ and quickly decrease to stabilize around $3.5\,\mathrm{kW{\cdot}m^{-2}}$ with a weak dispersion (minimum and maximum heat fluxes are also shown). Moreover, Figure 15d shows the estimated temperatures at the interface cast iron/dough. The weak dispersion of temperature shows a good repeatability of these three tests. The time integration of the estimated heat flux provides the energy per unit area transmitted by the cast iron. This energy (J) is compared with that deduced from an energy balance performed on the batter measurements, taking into account the sensible heat, the mass losses and the heat flux exchanged by radiation and convection with ambiance (equation (19)).

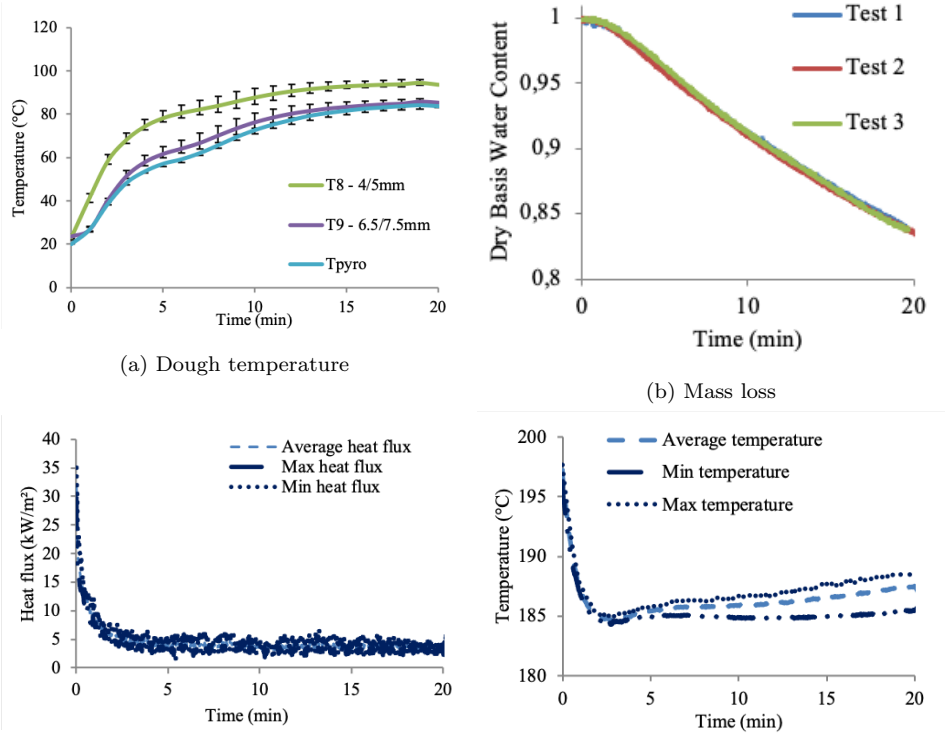

(a) Dough temperature

(b) Mass loss

(c) Heat flux estimation based T2 measurements

(d) Estimated surface temperature : average, minimum and maximum

Figure 15: Measurements and estimated results for three tests at 200 °C

$$\int \varphi(t)dtS_{surf} = -\Delta m L_v - h_{conv} S_{surf} \left(T_{pyrometer} - T_{amb}\right) - \epsilon\sigma S_{surf} \left(T^4_{pyrometer} - T^4_{amb}\right) + mc_p \left(T_{7,8,9} - T_0\right) \quad (19)$$

In this equation 19, the natural convection coefficient has been set at $6\,\mathrm{W{\cdot}m^{-2}{\cdot}K^{-1}}$. This value was deduced from relationships referenced in literature [29]. The emissivity of the cereal dough was measured using a Shimadzu UV-3600 spectrophotometer (ϵ= 0.9). The specific heat was calculated using the Baik & al. correlations [28] (see appendix A). The sensible heat was determined by decomposing the dough as 3 layers of 2 mm, 4 mm and 2 mm whose the temperatures were respectively T7, T8 and T9. The results are given in table 3.

In the case of a baking carried out at 170 °C, the total energy deduced from the fluxmeter measurements was equal to 70 kJ whereas the total energy calculated based on the equation 19 was 70 kJ (error inferior to 3 %). It can be assumed that there was a small heat loss between the energy calculated by the IHCP method and the incoming energy into the dough which demonstrate the reliability of the inverse method. This total energy was distributed as follows: 32 kJ related to the sensible heat, 27 kJ related to water vaporization and 9 kJ related to the heat exchanges with the ambiance (convection and radiation). Logically, the higher the heater temperature is, the greater the total energy transmitted to the dough is, for a similar baking duration. Thus, the total energy was 83 kJ at 200 °C and 105 kJ at 230 °C. The final dough temperatures being higher, the sensible heats were also greater. As mass losses increased with temperature, latent heat followed the same trend, as

did convection and radiation heat losses.

Table 3: Fluxmeter energy and total energy balance

Temperature (°C)	Fluxmeter energy (kJ)	Sensible heat (kJ)	Latent heat (kJ)	Convection/Radiation (kJ)	Total energy balance (kJ)
170	70	32	27	9	68
200	83	34	36	11	81
230	105	36	53	12	101

5. Conclusion

A method based on solving IHCPs was developed to estimate the heat flux transferred from a hot plate to a cold product during direct contact heating. This method was first developed and tested by numerical studies. A bi-dimensional numerical model was built to predict thermal phenomena during contact between a cold elastomer and a hot cast iron plate in the case of imperfect contact. The heat flux transmitted from the hot plate to the elastomer was directly deduced from this model. Two Inverse Heat Conduction Problems were developed and tested based on some temperatures of the hot plate and the elastomer. The two estimated heat flux obtained were compared with the direct model heat flux to validate the prescribed procedure. A sensitivity analysis was performed to quantify the impact of uncertainties (thermal properties and sensor locations) on the estimation and verify the robustness of the method.

Based on this numerical study, an experimental set-up was designed with adequate instrumentations. Experimental studies were first carried out for a contact hot plate / elastomer as numerically tested. The two heat flux estimated from elastomer temperatures on the one hand and from hot plate

temperatures on the other hand demonstrated the ability of the method to estimate an unknown heat flux. The procedure was next tested for the baking of a cereal dough. An energy balance conducted from temperatures measurements and mass losses measurements confirmed the value of total energy supplied to the dough deduced from the time integration of the estimated heat flux. Moreover, this energy balance provided a detailed distribution (sensible heat, water vaporization, convection and radiation heat losses) and participated to the total validation of the proposed method.

Appendix A

The thermal properties of the bakery product are estimated using the Baik & al. correlations [28]. These correlations depend on the mass fraction of each component (water, protein, carbohydrate, fat, fiber and ash): $c_p = \sum Y_i^W c_{p_i}$, $k = \sum Y_i^W k_i$, $\rho = \frac{1}{\sum \frac{Y_i^W}{\rho_i}}$. The composition of the dough are given in table 4.

Table 4: Dough composition

	Industrial preparation (%)	Milk (%)	Bakery product (%)
Protein	14.00	3.11	7.09
Carbohydrate	65.60	4.66	26.93
Fat	3.20	1.55	2.16
Fiber	3.70	0.00	1.35
Ash	1.20	0.24	0.59
Water	12.30	90.44	61.89

References

[1] Z.-F. Zhou, T.-Y. Xu, B. Chen, Algorithms for the estimation of transient surface heat flux during ultra-fast surface cooling, International Journal of Heat and Mass Transfer 100 (2016) 1–10.

[2] R. F. Brito, S. R. Carvalho, S. L. E. Silva, Experimental investigation of thermal aspects in a cutting tool using comsol and inverse problem, Applied Thermal Engineering 86 (2015) 60–68.

[3] S. K. Singh, M. K. Yadav, S. Khandekar, Measurement issues associated with surface mounting of thermopile heat flux sensors, Applied Thermal Engineering 114 (2017) 1105–1113.

[4] M. K. Yadav, S. K. Singh, A. Parwez, S. Khandekar, Inverse models for transient wall heat flux estimation based on single and multi-point temperature measurements, International Journal of Thermal Sciences 124 (2018) 307–317.

[5] J. R. Banga, Z. Pan, R. P. Singh, On the optimal control of contact-cooking processes, Food and Bioproducts Processing 79 (2001) 145–151.

[6] S. E. Zorrilla, R. P. Singh, Heat transfer in double-sided cooking of meat patties considering two-dimensional geometry and radial shrinkage, Journal of Food Engineering 57 (2003) 57–65.

[7] A. Putranto, X. D. Chen, W. Zhou, Modeling of baking of thin layer of cake using the lumped reaction engineering approach (L-REA), Journal of food engineering 105 (2011) 306–311.

[8] J. Cernela, B. Heyd, B. Broyart, Evaluation of heating performances and associated variability of domestic cooking appliances (oven-baking and pan-frying), Applied Thermal Engineering 62 (2014) 758–765.

[9] T. R. Gupta, Individual heat transfer modes during contact baking of Indian unleavened flat bread (chapati) in a continuous oven, Journal of Food Engineering 47 (2001) 313–319.

[10] G. Karimi, M. Feilizadeh, A. T. Najafabadi, Performance Analysis of Contact Baking of Flat Bread in an Indirect-Heating Oven, Drying technology 30 (2012) 1014–1023.

[11] R. S. Reddy, D. Arepally, A. Datta, Estimation of heat flux in bread baking by inverse problem, Journal of Food Engineering (2019) 109774.

[12] R. Rocca-Poliméni, N. Z. Vilet, S. Roux, J.-L. Bailleul, B. Broyart, Continuous measurement of contact heat flux during minced meat grilling, Journal of Food Engineering 242 (2019) 163 – 171.

[13] J. N. Rasera, K. J. Daun, C. J. Shi, M. D'Souza, Direct contact heating for hot forming die quenching, Applied Thermal Engineering 98 (2016) 1165–1173.

[14] T. Loulou, E. A. Artyukhin, J. P. Bardon, Estimation of thermal contact resistance during the first stages of metal solidification process: Iexperiment principle and modelisation, International Journal of Heat and Mass Transfer 42 (1999) 2119–2127.

[15] H. Massé, E. Arquis, D. Delaunay, S. Quilliet, P. H. Le Bot, Heat

transfer with mechanically driven thermal contact resistance at the polymer–mold interface in injection molding of polymers, International Journal of Heat and Mass Transfer 47 (2004) 2015–2027.

[16] T. Loulou, R. Abou-Khachfe, J.-P. Bardon, Estimation de la resistance thermique de contact durant la solidification du verre, International journal of thermal sciences 38 (1999) 984–998.

[17] J. V. Beck, Nonlinear estimation applied to the nonlinear inverse heat conduction problem, International Journal of heat and mass transfer 13 (1970) 703–716.

[18] J.-H. Noh, K.-U. Cha, S.-T. Ahn, S.-J. Yook, Prediction of time-varying heat flux along a hollow cylindrical tube wall using recursive input estimation algorithm and thermal resistance network method, International Journal of Heat and Mass Transfer 97 (2016) 232–241.

[19] J.-L. Bailleul, V. Sobotka, D. Delaunay, Y. Jarny, Inverse algorithm for optimal processing of composite materials, Composites Part A: Applied Science and Manufacturing 34 (2003) 695–708.

[20] D. Meresse, S. Harmand, M. Siroux, M. Watremez, L. Dubar, Experimental disc heat flux identification on a reduced scale braking system using the inverse heat conduction method, Applied Thermal Engineering 48 (2012) 202–210.

[21] P. Le Bideau, J. P. Ploteau, P. Glouannec, Heat flux estimation in an infrared experimental furnace using an inverse method, Applied Thermal Engineering 29 (2009) 2977–2982.

[22] F. Sanz-Serrano, C. Sagues, S. Llorente, Inverse modeling of pan heating in domestic cookers, Applied Thermal Engineering 92 (2016) 137–148.

[23] M. Raynaud, Le probleme inverse de conduction de la chaleur, Techniques de l'ingenieur. Génie énergétique 2 (1997) BE8265–1.

[24] D. W. Marquardt, An algorithm for least-squares estimation of nonlinear parameters, Journal of the society for Industrial and Applied Mathematics 11 (1963) 431–441.

[25] J.-H. Noh, W.-G. Kim, K.-U. Cha, S.-J. Yook, Inverse heat transfer analysis of multi-layered tube using thermal resistance network and kalman filter, International Journal of Heat and Mass Transfer 89 (2015) 1016 – 1023.

[26] Afnor. fonderie - fonte à graphite lamellaire. nf en 1561, 2011.

[27] F. P. Incropera, A. S. Lavine, T. L. Bergman, D. P. DeWitt, Fundamentals of heat and mass transfer, Wiley, 2007.

[28] O. D. Baik, M. Marcotte, S. S. Sablani, F. Castaigne, Thermal and physical properties of bakery products, Critical Reviews in Food Science and Nutrition 41 (2001) 321–352.

[29] A.-J. N. Khalifa, Natural convective heat transfer coefficient – a review: I. isolated vertical and horizontal surfaces, Energy Conversion and Management 42 (2001) 491 – 504.